Draft version January 5, 2007
Preprint typeset using LaTeX style emulateapj v. 10/09/06

HEMISPHERICAL POWER ASYMMETRY IN THE THREE-YEAR WILKINSON MICROWAVE ANISOTROPY PROBE SKY MAPS

H. K. Eriksen[1,2,3,4], A. J. Banday[5], K. M. Górski[3,4,6], F. K. Hansen[1,2] and P. B. Lilje[1,2]

Draft version January 5, 2007

ABSTRACT

We consider the issue of hemispherical power asymmetry in the three-year WMAP data, adopting the modulation framework introduced by Spergel et al. (2006), with some improvements and extensions. Important improvements include increased angular resolution, a more accurate likelihood definition, more natural parameter choices, and analysis of single-frequency maps, while the two extensions consist of the explicit evaluation of Bayesian evidence and the assessment of frequentist probabilities. With these tools, we find that the model consisiting of an isotropic CMB sky, modulated by a dipole field, gives a substantially better fit to the observations than the purely isotropic model does, even when including the penalty of a larger prior volume. For the ILC map, the Bayesian log-evidence difference is ~ 1.8 in favour of the modulated model, and the raw improvement in maximum log-likelihood is 6.1. The best-fit modulation dipole axis points toward $(l, b) = (225°, -27°)$, and the modulation amplitude is 0.114, in excellent agreement with the results from the first-year analyses. The frequentist probability of obtaining such a high modulation amplitude in an isotropic universe is $\sim 1\%$. These results are not sensitive to data set or sky cut. In conclusion, the statistical evidence for a power asymmetry anomaly is both substantial and robust, although not decisive, for the currently available data. Increased sky coverage through better foreground handling and full-sky and high-sensitivity polarization maps may shed further light on this issue.

Subject headings: cosmic microwave background — cosmology: observations — methods: statistical

1. INTRODUCTION

While the first-year results from the Wilkinson Microwave Anisotropy Probe (WMAP) experiment (Bennett et al. 2003) overall clearly supported the currently popular inflationary cosmological model, describing a flat, isotropic and homogeneous universe seeded by Gaussian and adiabatic fluctuations, a disturbing number of unexpected anomalies on large scales were reported shortly after the public data release. Perhaps the three most important ones were: 1) alignments and symmetry features among low ℓ multipoles (de Oliveira-Costa et al. 2004; Eriksen et al. 2004a), 2) an apparent asymmetry in the distribution of fluctuation power in two opposing hemispheres (Eriksen et al. 2004b; Hansen et al. 2004), and 3) a peculiar cold spot in the southern hemisphere (Vielva et al. 2004; Cruz et al. 2005). All of these features were subsequently studied extensively by independent groups, and all remain unresolved to the present day.

In March 2006 the three-year WMAP results were released, prompting researchers to revisit the anomalies detected in the first-year data (Bridges et al. 2006; Copi et al. 2006; Jaffe et al. 2006; Land & Magueijo 2006; Martínez-González et al. 2006). Of course, considering that already the first-year data were strongly signal-dominated on the scales of interest, it should come as no surprise that most of these analyses concluded with similar results as for the previous data, although different foreground handling could affect some results.

The WMAP team paid particular attention to the question of large-scale power asymmetry in their analyses. Specifically, Spergel et al. (2006) approached this problem from a semi-Bayesian point of view, by defining a parametric model consisting of an isotropic and Gaussian CMB field modulated by a large-scale function. The power asymmetry anomaly was addressed by a dipolar modulation field, and the low-ℓ alignment anomalies were studied with a quadrupole modulation field. They then asked: Is the likelihood improvement gained by this complication sufficient to justify the additional degrees of freedom? Their conclusion was negative in both cases.

However, several questions may be raised regarding their analyses. First, as far as the low-ℓ alignment issue goes, it should be noted that this anomaly was claimed to be a quadrupole–octopole anomaly (de Oliveira-Costa et al. 2004), and not extending to higher multipoles. Hence, any analysis of this feature defined in real space is ill conceived, and we are therefore not considering this issue further in this Letter.

On the other hand, the hemispherical power asymmetry reported by Eriksen et al. (2004b) is clearly visible between $\ell = 2$ and 40, more than a decade in harmonic space, and this anomaly is therefore well suited for the formalism defined by Spergel et al. (2006). On this background, we revisit the power asymmetry issue in this Letter, but implement a number of improvements and extensions to the formalism. First of all, Spergel et al. (2006) performed their analysis with a pixel size of 7° pixels, which only allowed robust resolution of harmonic modes

Electronic address: h.k.k.eriksen@astro.uio.no
[1] Institute of Theoretical Astrophysics, University of Oslo, P.O. Box 1029 Blindern, N-0315 Oslo, Norway
[2] Centre of Mathematics for Applications, University of Oslo, P.O. Box 1053 Blindern, N-0316 Oslo, Norway
[3] Jet Propulsion Laboratory, 4800 Oak Grove Drive, Pasadena CA 91109
[4] California Institute of Technology, Pasadena, CA 91125
[5] Max-Planck-Institut für Astrophysik, Karl-Schwarzschild-Str. 1, Postfach 1317, D-85741 Garching bei München, Germany
[6] Warsaw University Observatory, Aleje Ujazdowskie 4, 00-478 Warszawa, Poland

up to $\ell \sim 20$. We perform our analysis with 3.6° pixels, and thereby include structure up to $\ell \sim 40$. Second, the likelihood used by Spergel et al. (2006) was poorly defined with respect to the Nyquist limit (Eriksen et al. 2006), and this is corrected in the present analysis. Third, we replace the "χ^2 improvement per additional parameter" arguments of Spergel et al. (2006) by explicit computations of the Bayesian evidence.

2. ALGORITHMS

We now outline the methods used for the analyses presented in the following sections. The overall philosophy is identical to that of Spergel et al. (2006), but the implementational details are closer to those of Eriksen et al. (2006) and Mukherjee et al. (2006).

2.1. *Data model and likelihood*

Following Spergel et al. (2006), we model the CMB temperature sky maps as

$$\mathbf{d}(\hat{\mathbf{n}}) = \mathbf{s}(\hat{\mathbf{n}})[1 + f(\hat{\mathbf{n}})] + \mathbf{n}(\hat{\mathbf{n}}), \tag{1}$$

where $\mathbf{s}(\hat{\mathbf{n}})$ is a statistically isotropic and Gaussian random field with power spectrum C_ℓ, $f(\hat{\mathbf{n}})$ is a dipole modulation field with amplitude less than unity, and $\mathbf{n}(\hat{\mathbf{n}})$ is instrumental noise. Thus, the modulated signal component is an anisotropic, but still Gaussian, random field, and therefore has a covariance matrix given by

$$\tilde{\mathbf{S}}(\hat{\mathbf{n}}, \hat{\mathbf{m}}) = [1 + f(\hat{\mathbf{n}})]\mathbf{S}(\hat{\mathbf{n}}, \hat{\mathbf{m}})[1 + f(\hat{\mathbf{m}})], \tag{2}$$

where

$$\mathbf{S}(\hat{\mathbf{n}}, \hat{\mathbf{m}}) = \frac{1}{4\pi}\sum_\ell (2\ell + 1)C_\ell P_\ell(\hat{\mathbf{n}} \cdot \hat{\mathbf{m}}). \tag{3}$$

Taking into account instrumental noise and possible foreground contamination, the full covariance matrix is

$$\mathbf{C}(\hat{\mathbf{n}}, \hat{\mathbf{m}}) = \tilde{\mathbf{S}}(\hat{\mathbf{n}}, \hat{\mathbf{m}}) + \mathbf{N} + \mathbf{F}. \tag{4}$$

The noise and foreground covariance matrices depend on the data processing, and will be described in greater detail in §3.

With these definitions ready at hand, the log-likelihood is given by

$$-2\log\mathcal{L} = \mathbf{d}^T\mathbf{C}^{-1}\mathbf{d} + \log|\mathbf{C}|, \tag{5}$$

up to an irrelevant constant. Note that our definitions differ slightly from those of Spergel et al. (2006), in that we take into account the (unmodulated) noise and foreground terms.

2.2. *Posterior distributions and choice of parameters*

The posterior distribution $P(\theta|\mathbf{d})$ is a primary goal of any Bayesian analysis, θ being the set of all free parameters in the model. For the model defined above, the free parameters can be divided into two groups, namely those describing the isotropic CMB covariance matrix or C_ℓ, and those describing the modulation field. Both may be parametrized in a number of different ways, and these choices may affect the outcome of the analysis through different prior definitions.

We are mostly interested in the properties of the modulation field in this paper, and the isotropic CMB component is therefore of less consequence. Spergel et al. (2006) chose to sample each C_ℓ, $\ell = 0, \ldots, 10$, individually, but fixed the higher ℓ's at their best-fit values. For computational efficiency reasons, we choose instead a simple two-parameter model with free amplitude q and tilt n,

$$C_\ell = q\left(\frac{\ell}{\ell_0}\right)^n C_\ell^{\rm fid}. \tag{6}$$

Here ℓ_0 is a pivot multipole and $C_\ell^{\rm fid}$ is a fiducial model, in the following chosen to be the best-fit power law spectrum of Hinshaw et al. (2006).

The choice of parameters for the modulation field is more subtle. Spergel et al. (2006) simply used standard spherical harmonics coefficients $a_{\ell m}$ for this purpose. We prefer a more intuitive set of parameters, namely a direction $\hat{\mathbf{p}}$ and an overall amplitude A,

$$f(\hat{\mathbf{n}}) = A\,\hat{\mathbf{n}} \cdot \hat{\mathbf{p}}. \tag{7}$$

The difference between the two choices lies primarily in prior volume definition, which is of less importance for parameter estimation, but crucial for evidence computations[7].

We use flat priors on all parameters in this paper; the modulation axis is uniform over the sphere, and the amplitude is restricted to $A \leq 0.3$. The power spectrum parameters are restricted to $0.5 \leq q \leq 1.5$ and $-0.5 \leq n \leq 0.5$. These choices are sufficiently generous to include all non-zero parts of the likelihood.

The posterior distribution,

$$P(q, n, A, \hat{\mathbf{p}}|\mathbf{d}) \propto \mathcal{L}(q, n, A, \hat{\mathbf{p}})P(q, n, A, \hat{\mathbf{p}}), \tag{8}$$

is then mapped out using a standard Markov Chain Monte Carlo technique. We use a Gaussian proposal density for q, n, and A, and an Euler-matrix based, uniform proposal density for $\hat{\mathbf{p}}$.

2.3. *Bayesian evidence and nested sampling*

In a Bayesian analysis, one is not only interested in the set of best-fit parameter values, but also in the relative probability of competing models. The most direct way of measuring this is through the Bayesian evidence,

$$E \equiv P(\mathbf{d}|H) = \int P(\mathbf{d}|\theta, H)P(\theta|H)d\theta, \tag{9}$$

which is simply the average likelihood over the prior volume. Typically, one computes this quantity for two competing models, H_0 and H_1, and considers the difference $\Delta\log E = \log E_1 - \log E_0$. If $\Delta\log E > 1$, the evidence for H_1 is considered substantial; if $\Delta\log E > 2.5$, it is considered strong.

Traditionally, computation of evidences has been a computational challenge. However, Mukherjee et al. (2006) introduced a method called "nested sampling", proposed by Skilling (2004), to the cosmological community that allows for accurate estimation of the evidence through Monte Carlo sampling. We implemented this for the priors and likelihood described above, and found that it works very well for the problem under consideration.

[7] Using polar coordinates, a uniform prior implies equal weighting of all directions on the sky, while with cartesian (or harmonics) coordinates, some directions would be preferred unless special care is taken.

TABLE 1

Data	$(l_{\rm bf}, b_{\rm bf})$	$A_{\rm bf}$	$\Delta \log \mathcal{L}$	$\Delta \log E$	P
ILC[a]	$(225°, -27°)$	0.114	6.1	1.8 ± 0.2	0.991
ILC[b]	$(208°, -27°)$	0.125	6.0	1.8 ± 0.2	0.991
Q-band[b]	$(222°, -35°)$	0.124	5.5	1.5 ± 0.2	0.987
V-band[b]	$(205°, -19°)$	0.127	5.6	1.5 ± 0.2	0.990
W-band[b]	$(204°, -31°)$	0.121	5.2	1.3 ± 0.2	0.985
WMAP[a,c]	$(204°, -30°)$	0.103	1.7	N/A	N/A

NOTE. — Modulation model results. The listed quantities are the marginal best-fit dipole axis (*second column*) and amplitude (*third column*); the change in likelihood at the posterior maximum, $\Delta \log \mathcal{L} = \log \mathcal{L}_{\rm mod} - \log \mathcal{L}_{\rm iso}$, between the modulated and the isotropic model (*fourth column*); the Bayesian evidence difference, $\Delta \log E = \log E_{\rm mod} - \log E_{\rm iso}$ (*fifth column*); and the frequentist probability for obtaining a lower maximum-likelihood modulation amplitude than the observed one, computed from isotropic simulations (*sixth column*).
[a] Liberal 12.8% sky cut imposed.[b] Conservative 36.3% sky cut imposed.[c] As presented by Spergel et al. (2006).

2.4. *Maximum-likelihood analysis*

We also perform a standard frequentist maximum-likelihood analysis by computing the maximum-likelihood modulation parameters for isotropic Monte Carlo simulations. For these computations, we use a modified version of the evidence code, which we find to be considerably more robust than a simple non-linear search; while the non-linear search algorithms often get trapped in local minima, the nested sampling algorithm always find the correct solution, but of course, at a considerably higher computational expense.

3. DATA

We analyze two versions of the three-year WMAP sky maps in the following; the template-corrected Q-, V-, and W-band maps, and the "foreground cleaned" Internal Linear Combination (ILC) map (Hinshaw et al. 2006). All maps are processed as described by Eriksen et al. (2006): They are first downgraded to HEALPix[8] resolution $N_{\rm side} = 16$, by additional smoothing to a 9° FWHM Gaussian beam and appropriate pixel window. Second, uniform Gaussian noise of $\sigma_{\rm n} = 1\,\mu$K is added to each pixel in order to regularize the pixel-pixel covariance matrix. This combination of smoothing and noise level results in a signal-to-noise ratio of unity at $\ell = 40$, and strong noise domination at the Nyquist multipole of $\ell = 47$.

We use two different sky cuts for our analyses. First, given that the galactic plane is clearly visible in the single frequency data, our first mask is conservatively defined. This cut is created by expanding the Kp2 mask Hinshaw et al. (2006) by 9° in all directions, and then manually removing all near-galactic pixels for which any difference map between two channels are clearly larger than noise. In total, 36.3% of all pixels are rejected by this cut (see figure 2). Second, we also adopt the directly downgraded Kp2 cut used by the WMAP team that removes 12.8% of all pixels. We use this mask for the ILC map only.

The noise covariance matrix is given by the uniform noise only, $N_{ij} = \sigma_{\rm n}^2 \delta_{ij}$. For completeness, we have also computed the noise covariance from the smoothed instrumental noise for the V-band data, but we find that this has no effect on the final results, since its amplitude is far below the CMB signal. It is therefore omitted in the following.

As an additional hedge against foreground contamination, we marginalize over a set of fixed spatial templates, $\mathbf{t}_i$, through the covariance matrix $\mathbf{F}_i = \alpha_i \mathbf{t}_i \mathbf{t}_i^T$, $\alpha_i \gtrsim 10^3$. Monopole and dipole terms are always included, and one or more foreground templates. For the V-band and ILC maps, we follow Hinshaw et al. (2006) and adopt V–ILC as our foreground template. For the Q-band data, we marginalize over a synchrotron (Haslam et al. 1982), a free-free (Finkbeiner 2003), and a dust (Finkbeiner et al. 1999) template individually. Finally, for the W-band data, we use the W–ILC difference map. However, we have tried various combinations for all maps, and there is virtually no sensitivity to the particular choice, or indeed, to the template at all, due to the conservative sky cut used.

[8] http://healpix.jpl.nasa.gov

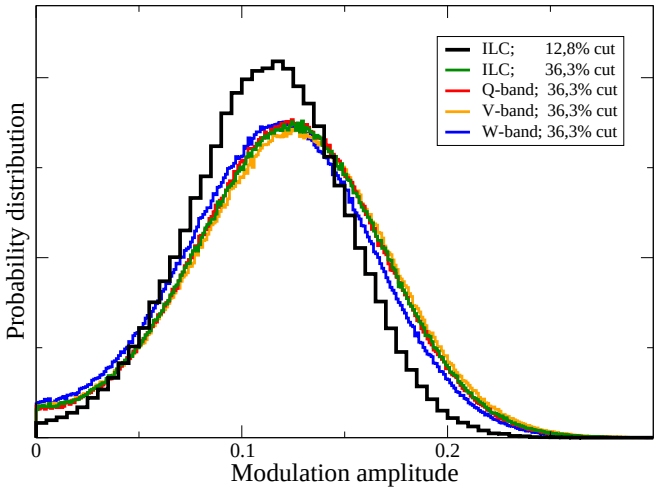

FIG. 1.— Posterior distributions for the dipole modulation amplitude, marginalized over direction and CMB power spectrum.

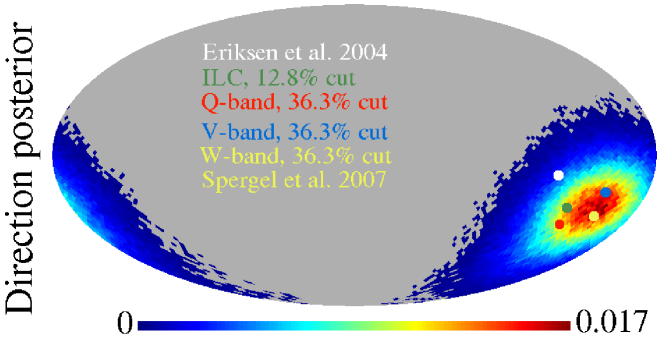

FIG. 2.— Posterior distribution for the dipole modulation axis, shown for the ILC map and 36.3% sky cut, and marginalized over power spectrum and amplitude parameters. Grey sky pixels indicate pixels outside the 2σ confidence region. The dots indicate the axis 1) reported by Eriksen et al. (2004) in white; 2) for the ILC map with a 12.8% sky cut in green; 3) for the Q-, V-, and W-bands in red, blue and yellow, respectively. The axis reported by Spergel et al. (2006) coincides with the W-band axis.

4. RESULTS

The results from the analysis outlined above are summarized in Table 1. For each map, we report the best-fit dipole axis and amplitude, as well as the maximum log-

likelihood difference and Bayesian evidence difference for the modulated versus the isotropic model. The errors on the evidence are estimated by performing eight independent analyses for each case, and computing the standard deviation (Mukherjee et al. 2006). We also compute the probability of obtaining a smaller modulation amplitude than the observed one by analyzing 1000 isotropic Monte Carlo simulations.

Starting with the case considered by Spergel et al. (2006), namely the ILC map cut by a 12.8% mask, we find that the best-fit modulation axis points toward $(l, b) = (225^\circ, -27^\circ)$, and the corresponding amplitude is 0.114. For comparison, the best-fit modulation spherical harmonics coefficients reported by Spergel et al. (2006) correspond to a best-fit axis of $(l, b) = (204^\circ, -30^\circ)$ and a modulation amplitude of 0.103. The agreement is thus quite good in terms of best-fit parameter values. However, there is nevertheless one very important difference between the two analyses: While Spergel et al. (2006) included angular scales only up to $\ell \lesssim 20$ in their analysis, our data are signal dominated up to $\ell \lesssim 40$. The fact that the best-fit parameters do not change despite adding three times more data[9] implies significantly smaller uncertainties around the same central values.

This translates into a higher total significance. Spergel et al. (2006) reported that the change in best-fit likelihood for their two models was $\Delta \log \mathcal{L} = 1.7$, which is quite insignificant given the addition of three new parameters. However, the corresponding number for the revised analysis is $\Delta \log \mathcal{L} = 5$ to 6, depending on data set. Further, the difference in *Bayesian evidence* is about $\Delta \log E = 1.5$ to 1.8. Thus, the result quoted by Spergel et al. (2006) is significantly under-estimated: Even after taking into account the prior penalty due to the additional parameters, the modulated model is five or six times more likely than the isotropic model. The probability of finding such a high modulation amplitude in isotropic simulations is $\sim 1\%$ (note that while the best-fit axis and amplitude listed in Table 1 are marginal values, the amplitude used in the frequentist test is the actual maximum-likelihood value).

These results are not particularly sensitive to data set or sky coverage, as seen in Table 1. In Figure 1 we show the marginalized posterior distributions for the modulation amplitudes for each data set, and also here we see that the agreement among data sets is very good.

In Figure 2 we show the dipole axis posterior distribution for the ILC map and 36.3% sky cut. Superimposed on this, we have also marked the first-year asymmetry axis reported by Eriksen et al. (2004b) $[(l, b) = (237^\circ, -10^\circ)]$ in white, and also the other axes listed in Table 1. All agree well within 2σ, and this is an excellent testimony to the stability of the effect with respect to statistical method, data set and overall procedure.

Finally, we note that this model may also partially explain the anomalous cold spot reported by Vielva et al. (2004) and Cruz et al. (2005): By demodulating the map, the spot would increase its temperature by about 10%. Although still very cold, it would be significantly less extreme. Similar arguments could possibly also be made for the Bianchi VII_h correlation found by Jaffe et al. (2005). These issues will be considered further in future work.

5. CONCLUSIONS

A notable power asymmetry between two opposing hemispheres in the first-year WMAP sky maps was reported by Eriksen et al. (2004b). This feature may be observed as strong fluctuations in the southern ecliptic hemisphere, but virtually no large-scale structure in the northern ecliptic hemisphere (e.g., Hinshaw et al. 2006).

In this Letter, we have revisited this issue in the three-year WMAP data, adopting the statistical framework introduced and applied by Spergel et al. (2006). While this framework is theoretically very appealing, having strong connections to well-established Bayesian theory, we find that the implementation of Spergel et al. (2006) can be improved. One important problem with the initial analysis was the limited angular range used. The power anomaly has previously been shown to extend up to $\ell \sim 40$, whereas Spergel et al. (2006) only considered scales up to $\ell \sim 20$. A second problem was their implementation of the likelihood, which employed harmonic modes beyond the Nyquist frequency in order to regularize the CMB covariance matrix (Eriksen et al. 2006).

Taking into account these issues, we find that the evidence for power asymmetry in the WMAP data is quite consistent with that initially reported for the first-year maps by Eriksen et al. (2004b); the WMAP data clearly suggest a dipolar distribution of power on the sky. The amplitude of modulation is roughly 12% in real space, or about 20% in terms of power spectra. The best-fit dipole direction is $(l, b) \sim (225^\circ, -27^\circ)$. All results are independent of data set choices, i.e., frequency channel or sky cut.

However, the statistical evidence for this effect is still only tentative. In frequentist language, the significance is about 99%, while in Bayesian terms, the log-evidence difference is ~ 1.5 to 1.8, corresponding to odds of one to five or six. This is quite comparable to the evidence for $n_{\mathrm{s}} \neq 1$ after the three-year WMAP data release, for which the odds are about one to eight in the highest case (Parkinson et al. 2006). Thus, there is still a chance that the effect may be a fluke, and most likely, this will remain the situation until Planck provides new data in some five years. With additional frequency coverage, a better job can be done on foreground treatment, and more sky coverage can be reliably included in the analysis. Second, full-sky and high-sensitivity polarization data should provide valuable insights on the origin of the effect.

HKE acknowledges financial support from the Research Council of Norway. Some of the results in this paper have been derived using the HEALPix (Górski et al. 1999) software and analysis package. We acknowledge use of the Legacy Archive for Microwave Background Data Analysis (LAMBDA). Support for LAMBDA is provided by the NASA Office of Space Science.

[9] The information content of a random field defined on a sphere scales as $O(\ell^2)$.

REFERENCES

Bennett, C. L., et al. 2003, ApJS, 148, 1

Bridges, M., McEwen, J. D., Lasenby, A. N., & Hobson, M. P. 2006, [astro-ph/0605325]

Copi, C. J., Huterer, D., Schwarz, D. J., & Starkman, G. D. 2006, [astro-ph/0605135]

Cruz, M., Martínez-González, E., Vielva, P., & Cayón, L. 2005, MNRAS, 356, 29

de Oliveira-Costa, A., Tegmark, M., Zaldarriaga, M., & Hamilton, A. 2004, Phys. Rev. D, 69, 063516

Eriksen, H. K., Banday, A. J., Górski, K. M., & Lilje, P. B. 2004a, ApJ, 612, 633

Eriksen, H. K., Hansen, F. K., Banday, A. J., Górski, K. M., & Lilje, P. B. 2004b, ApJ, 605, 14

Eriksen, H. K., et al. 2006, ApJ, in press, [astro-ph/0606088]

Finkbeiner, D.P., Davis, M., & Schlegel, D.J. 1999, ApJ, 524, 867

Finkbeiner, D. P. 2003, ApJS, 146, 407

Hansen, F. K., Banday, A. J., & Górski, K. M. 2004, MNRAS, 354, 641

Haslam, C. G. T., Salter, C. J., Stoffel, H., & Wilson, W. 1982, A&AS, 47, 1

Hinshaw, G., et al. 2006, ApJ, submitted, [astro-ph/0603451]

Jaffe, T. R., Banday, A. J., Eriksen, H. K., Górski, K. M., & Hansen, F. K. 2005, ApJ, 629, L1

Jaffe, T. R., Banday, A. J., Eriksen, H. K., Górski, K. M., & Hansen, F. K. 2006, A&A, 460, 393

Land, K., & Magueijo, J. 2006, MNRAS, submitted, [astro-ph/0611518]

Martínez-González, E., Cruz, M., Cayón, L., & Vielva, P. 2006, New Astronomy Review, 50, 875

Mukherjee, P., Parkinson, D., & Liddle, A. R. 2006, ApJ, 638, L51

Parkinson, D., Mukherjee, P., & Liddle, A. R. 2006, Phys. Rev. D, 73, 123523

Skilling, J. 2004, in AIP Conf. Proc. 735, Bayesian Inference and Maximum Entropy Methods in Science and Engineering. ed. R. Fischer, R. Preuss,& U. von Toussaint (Melville: AIP), 395

Spergel, D. N., et al. 2006, ApJ, submitted, [astro-ph/0603449]

Vielva, P., Martínez-González, E., Barreiro, R. B., Sanz, J. L., & Cayón, L. 2004, ApJ, 609, 22